Human Molecular Genetics, 2021, Vol. 30, No. 21 1907–1918

https://doi.org/10.1093/hmg/ddab157
Advance Access Publication Date: 8 June 2021
General Article

GENERAL ARTICLE

Transcript isoforms of Reep6 have distinct functions in the retina

Qingnan Liang[1,2,*], Nathaniel Wu[1,*], Smriti Zaneveld[1], Hehe Liu[1], Shangyi Fu[1], Keqing Wang[1], Renae Bertrand[1,2], Jun Wang[1], Yumei Li[1] and Rui Chen[1,2,*]

[1]Human Genome Sequencing Center, Department of Molecular and Human Genetics, Baylor College of Medicine, Houston, TX 77030, USA and [2]Verna and Marrs McLean Department of Biochemistry and Molecular Biology, Baylor College of Medicine, Houston, TX, 77030 USA

*To whom correspondence should be addressed at: N1519, Baylor College of Medicine, One Baylor Plaza, Houston, TX 77030, USA. Tel: +1-7137985194; Fax: +1-7137985194; Email: ruichen@bcm.edu

Abstract

Much of the complexity of the eukaryotic cell transcriptome is due to the alternative splicing of mRNA. However, knowledge on how transcriptome complexity is translated into functional complexity remains limited. For example, although different isoforms of a gene may show distinct temporal and spatial expression patterns, it is largely unknown whether these isoforms encode proteins with distinct functions matching their expression pattern. In this report, we investigated the function and relationship of the two isoforms of *Reep6*, namely *Reep6.1* and *Reep6.2*, in rod photoreceptor cells. These two isoforms result from the alternative splicing of exon 5 and show mutually exclusive expression patterns. *Reep6.2* is the canonical isoform that is expressed in non-retinal tissues, whereas *Reep6.1* is the only expressed isoform in the adult retina. The *Reep6.1* isoform-specific knockout mouse, $Reep6^{E5/E5}$, is generated by deleting exon 5 and a homozygous deletion phenotypically displayed a rod degeneration phenotype comparable to a *Reep6* full knockout mouse, indicating that the *Reep6.1* isoform is essential for the rod photoreceptor cell survival. Consistent with the results obtained from a loss-of-function experiment, overexpression of *Reep6.2* failed to rescue the rod degeneration phenotype of *Reep6* knockout mice whereas overexpression of *Reep6.1* does lead to rescue. These results demonstrate that, consistent with the expression pattern of the isoform, *Reep6.1* has rod-specific functions that cannot be substituted by its canonical isoform. Our findings suggested that a strict regulation of splicing is required for the maintenance of photoreceptor cells.

Introduction

Alternative splicing allows for different mature mRNAs to be synthesized from a single precursor mRNA, resulting in multiple protein isoforms of mRNAs and increasing the functional diversity of each gene. It has been shown that 95% of multi-exon genes are involved in the alternative splicing process (1). Potential factors that lead to the functional differences among protein isoforms include changed protein localization, altered functional domains and reformed protein–protein interaction networks (2–4). The process of alternative splicing requires the spliceosome, a complex made up of core ribonucleoproteins and auxiliary proteins, to accurately recognize the splicing site and catalyze the reaction (5,6). Many tissue-specific features, including the expression of tissue-specific splicing regulatory proteins, or expression levels of the ubiquitously expressed splicing factors, affect the splicing process and thus lead to the synthesis of tissue-specific protein isoforms (7–9).

Besides tissue specificity, multiple splicing isoforms are switched temporally during development. Developmentally regulated expression of splicing regulators reportedly shapes

Received: March 16, 2021. **Revised:** May 30, 2021. **Accepted:** May 31, 2021

mRNA splicing in heart and brain development (10,11). For example, RNA binding proteins Rbfox and Ptbp1 are critical for cell fate decisions in the developing cerebral cortex by controlling the switching of protein isoforms, especially the isoforms of *Nin* and *Flna* (12). Different Nin isoforms showed distinct cell localization, which contribute to the differentiation of neuron progenitor cells. Also, the isoform switching of *Shtn1* was reported to regulate early axonogenesis in neurons, regulated by RNA binding protein Ptpb2 (13). The roles of tissue-specific and temporal-related splicing indicate the potential cell-specific importance for targets that undergo isoform switching.

The Receptor Expression-Enhancing Protein 6 gene (*REEP6*) is a gene whose isoforms exhibit temporally and spatially distinct expression patterns during retina development and is a member of the Yop1/Yip family, which has been implicated with the enhancement of cell surface expressions and endoplasmic reticulum membrane shaping (14). Harmful mutations in *REEP6* could lead to rod photoreceptor cell degeneration in both humans and mice (15–17). In previous studies (15,17), we generated *Reep6*$^{-/-}$ mice and evaluated their visual phenotype. We showed that the outer nuclear layers (ONLs) of the Reep6$^{-/-}$ mice were thinned compared with the *Reep6*$^{+/-}$ genotype, detectable as early as 20 days postnatal. Scotopic electroretinogram (ERG) recording also showed a rod photoreceptor defect in Reep6$^{-/-}$ mice, which was consistent with the histology features. *Reep6*$^{+/-}$ mice showed no differences with wild type mice in both histology and ERG recordings. These mice strains were also used in our current study.

There are two *REEP6* transcription isoforms observed, *REEP6.1* and REEP6.2. The noncanonical isoform of REEP6 protein (termed REEP6.1) contains a 27-amino-acids region encoded by the inclusion of Exon 5 of the *REEP6* gene. Mouse Reep6.1 protein was first reported to be highly expressed in the retina (18). Further studies confirmed that *REEP6.1* is also a major isoform expressed in the human retina while the canonical *REEP6* isoform, termed *REEP6.2*, has very low expression in adult human and mouse retinas (15,18). However, whether the tissue-specific expression pattern of these two isoforms is correlated with their function is not known.

Based on the mutually exclusive expression pattern of the two isoforms in the retina, we hypothesize that the *REEP6.1* isoform plays a role in the retina that is distinct from that of *REEP6.2*. However, it is possible that, despite their differences in expression patterns, the two isoforms are functionally interchangeable, since they only differ by 27 amino acids that are not highly conserved during evolution. To test these two competing hypotheses, a *Reep6.1* isoform-specific knockout mouse was generated by deleting Exon 5 (*Reep6*^{E5}). Together with the *Reep6*$^{-/-}$ mouse (*Reep6* full knockout) reported by our lab previously (17,19), we evaluated the retinal phenotype of *Reep6*$^{E5/+}$, *Reep6*$^{E5/E5}$ and *Reep6*$^{E5/-}$ mutant mice. Immunohistochemistry experiments confirmed that Reep6.2 was expressed in *Reep6*$^{E5/E5}$ and *Reep6*$^{E5/-}$ mice, with the same cellular localization as Reep6.1. Functional and histology characterization of the retina of the *Reep6*$^{E5/E5}$ and *Reep6*$^{E5/-}$ mice indicate that both mutant mice exhibited degeneration as severe as *Reep6*$^{-/-}$ mice, at 16 weeks old. Moreover, overexpression of *Reep6.1* could rescue the rod degeneration phenotype in *Reep6*$^{-/-}$ mice, whereas *Reep6.2* could not. Taken together, we conclude that in the retina, the retinal specific isoform *Reep6.1* cannot be functionally substituted by its canonical isoform, *Reep6.2*.

Results

REEP6.1 is the major *REEP6* isoform in adult human retina

The *REEP6* gene encodes two mRNA isoforms that differ by one exon, the fifth exon (Fig. 1A). We first investigated the expression of the two isoforms in different human tissues (Fig. 1B). In the adult retina, the mRNA with exon 5 was expressed, indicated by the signals in exon 5 region. There were also exon 5 signals in human frontal cortex and cerebral cortex, whereas the signals were relatively lower than the other exons, indicating a mixture of two isoforms in the brain tissues. In other tissues including muscle, skin and blood, etc., RNA-seq data showed that REEP6.2 was the major isoform, if not the sole isoform.

Generation of *Reep6.1* isoform-specific knock out mice

To generate a *Reep6.1* isoform-specific germline knockout, the exon 5 of *Reep6* was deleted using the CRISPR-Cas9 technology. As was shown in Figure 1C, two guide RNAs (gRNAs) flanking exon 5 were synthesized and injected along with Cas9 RNA into the mouse blastocyst to induce a deletion of the allele containing 420 base pairs (bp), including the entire exon 5, and the resulting mutant was named *Reep6*^{E5}. Founder mice carrying the E5 deletion were selected and crossed to a wild-type mice to establish stable germline deletion colonies. Homozygous *Reep6*$^{E5/E5}$ mutant mice were obtained, which showed normal viability and fertility with no observable gross defect through examination.

To assess the expression pattern of the two *Reep6* isoforms, reverse transcription PCR (RT-PCR) was performed using retinal RNA from *Reep6*$^{E5/E5}$, *Reep6*$^{E5/+}$ and *Reep6*$^{+/-}$ as a control. As shown in Figure 1D, in the *Reep6*$^{+/-}$ control retina, *Reep6.1* isoform is highly expressed with little *Reep6.2* isoform detected. In contrast, only *Reep6.2* isoform is detected in the *Reep6*$^{E5/E5}$ retina. Furthermore, both isoforms are detected in the *Reep6*$^{E5/+}$ retina. Similarly, western blot was performed to validate whether the two protein isoforms were expressed among these lines consistently with their mRNA pattern (Fig. 1E). As a result, we observed that only Reep6.1 was expressed in *Reep6*$^{+/-}$ retina, whereas only Reep6.2 was expressed in *Reep6*$^{E5/E5}$ and *Reep6*$^{E5/-}$ retina. Two bands indicating both isoforms were detected in *Reep6*$^{E5/+}$ retina. Therefore, we confirmed that, with exon 5 deleted, the *Reep6*^{E5} allele abolishes Reep6.1 expression and switches to express the *Reep6.2* isoform in the retina.

To further examine if Reep6 protein is produced by the *Reep6*^{E5} allele and if the *Reep6.2* isoform protein has similar subcellular localization as *Reep6.1* protein in the retina, immunofluorescent (IF) staining was performed (Fig. 2A–F). In *Reep6*$^{E5/E5}$ and *Reep6*$^{E5/-}$ retina, only *Reep6.2* isoform is produced, and Reep6 protein is primarily detected in the inner segment of the photoreceptor cells with a low level of protein observed in the perinuclear region. This pattern is the same as that of Reep6.1, as observed in the *Reep6*$^{+/-}$ and *Reep6*$^{+/+}$ retina (Fig. 2A). Furthermore, consistent with the wild type allele, no Reep6 signals could be detected in the inner nuclear and ganglion cell retinal layers in the *Reep6*$^{E5/E5}$ retina, indicating that the *Reep6*^{E5} allele shows photoreceptor cell-specific expression. Finally, we quantified the protein levels of Reep6 in the retina by western blot for all six genotypes, and all mice were 6-week old (Fig. 2G). We found that the *Reep6*$^{+/+}$, *Reep6*$^{E5/+}$ and *Reep6*$^{E5/E5}$ retina showed no different levels of Reep6 protein. The *Reep6*$^{E5/+}$ showed the highest expression level of Reep6, which is higher than *Reep6*$^{+/-}$,

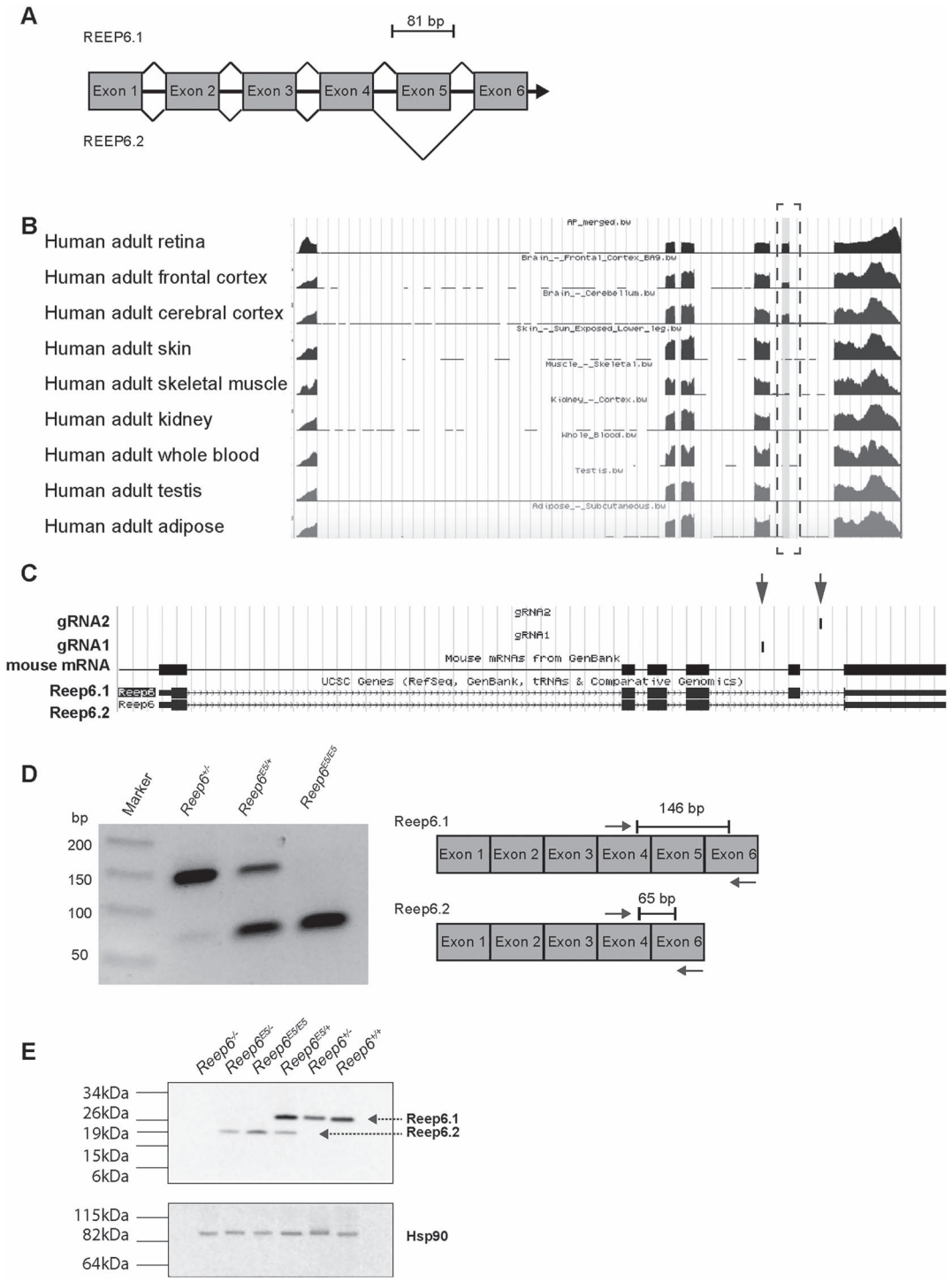

Figure 1. Overview of the two splicing isoforms of *REEP6* and the production of the exon KO mice. (**A**) Schematic showing two splicing isoforms of *REEP6*. (**B**) Visualization of RNA-seq peaks within human *REEP6* gene from different tissues. The alternative exon, exon 5, was highlighted with a dashed box. (**C**) Visualization of the relative positions of the two gRNAs in the mouse *Reep6* gene. (**D**) RT-PCR showing distinguishable band position for Reep6.1 and Reep6.2 mRNA. (**E**) Western blot experiment showing distinguishable band position for Reep6.1 and Reep6.2 protein species. From left to right, retina protein extracts from $Reep6^{-/-}$, $Reep6^{E5/-}$, $Reep6^{E5/E5}$, $Reep6^{E5/+}$, $Reep6^{+/-}$ *and* $Reep6^{+/+}$ were loaded. Hsp90 was used as a loading control. Dashed line with arrows highlighted the band of molecular weight of Reep6.1 or Reep6.2 proteins.

whereas $Reep6^{+/+}$ or $Reep6^{E5/E5}$ retina did not show a higher Reep6 level than $Reep6^{+/-}$ with statistical significance. The $Reep6^{E5/-}$ retina had a lower Reep6 level than the $Reep6^{+/+}$, $Reep6^{E5/+}$ and $Reep6^{E5/E5}$ retina, but not a statistically lower Reep6 level than the $Reep6^{+/-}$. Thus, we confirmed that the $Reep6^{E5}$ allele specifically affect mRNA splicing of the Reep6.1 isoform while it has little effect on the overall transcription of the *Reep6* gene. Therefore, in combination with *Reep6* knockout mice, the $Reep6^{E5}$ allele allowed us to distinguish the function of *Reep6*.1 and *Reep6*.2 isoform *in vivo*.

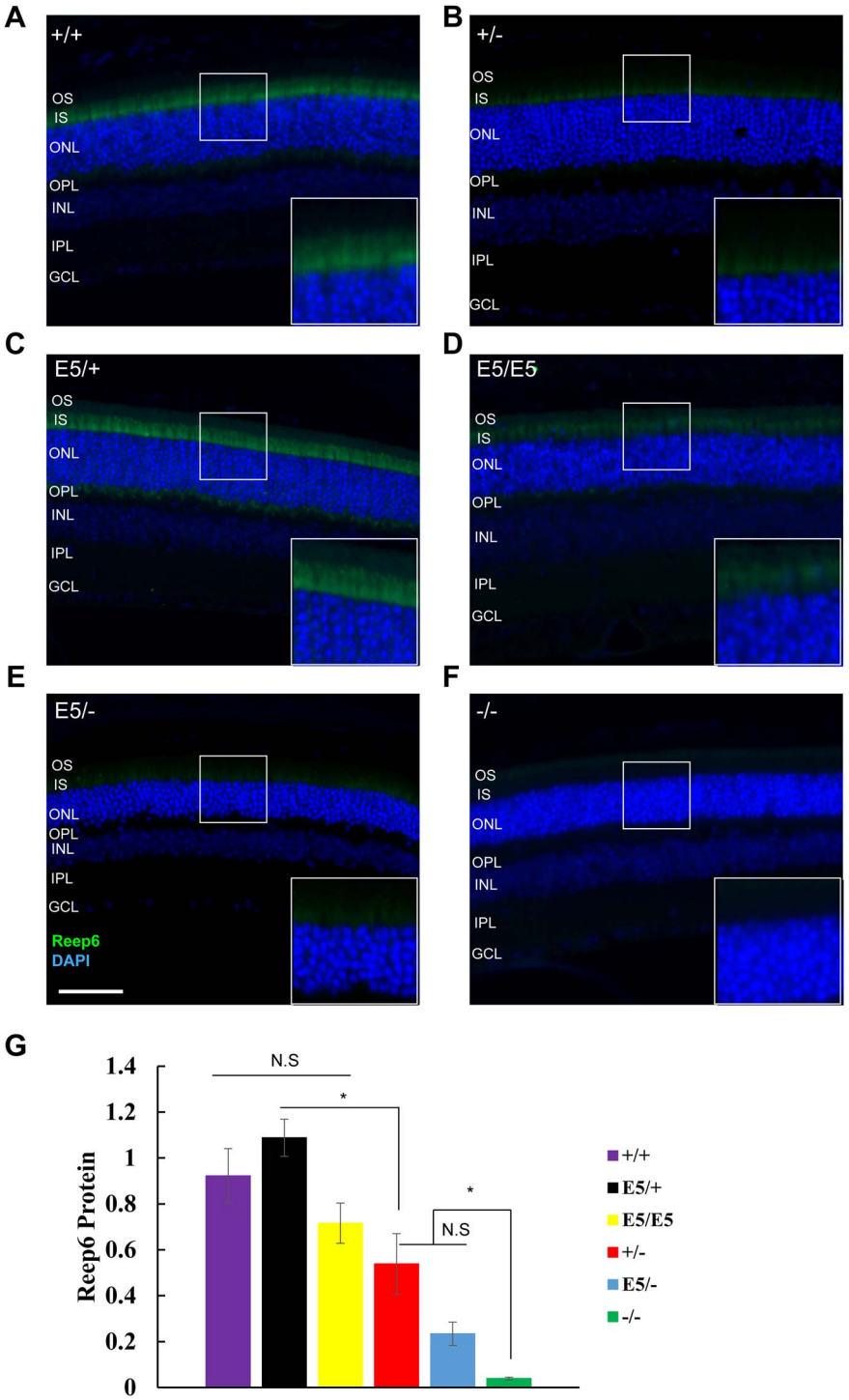

Figure 2. Confirmation of Reep6.2 expression in *Reep6*^{E5} mouse strains. **(A–F)** Immunofluorescence staining for Reep6 in the retina of *Reep6*$^{+/+}$, *Reep6*$^{+/-}$, *Reep6*$^{E5/+}$, *Reep6*$^{E5/E5}$, *Reep6*$^{E5/-}$ and *Reep6*$^{-/-}$, respectively. White rectangles highlight a zoomed view for protein expression. The scale bar represents 50 micrometers. Please note that the sections used for IF staining and quantification were not strictly selected at the very middle of the retina, thus could not represent the thickest part of the retina of each genotype (shown in Fig. 4). **(G)** Quantification of relative protein level from the western blot. For each mouse strains, four biological replicates were used, except *Reep6*$^{-/-}$ (three). The measurement of protein level was the ratio between the Reep6 signal and the control of the same lane.

Reep6 $^{E5/E5}$ and *Reep6*$^{E5/-}$ models exhibit visual defects

To characterize the phenotype of the *Reep6*$^{E5/+}$, *Reep6*$^{E5/E5}$ and *Reep6*$^{E5/-}$ retina, full-field ERG recording to measure the photoreceptor function of dark-adapted mice was performed. *Reep6*$^{+/-}$ and *Reep6*$^{-/-}$ mice were used as controls. Two time points, 4 weeks and 16 weeks postnatal, were selected for this measurement. For both scotopic a-wave and b-wave at both time points, the wave amplitudes for *Reep6*$^{E5/-}$ was at the same level as *Reep6*$^{-/-}$, both of which showed a significant decrease compared with *Reep6*$^{E5/+}$ and *Reep6*$^{+/-}$ (Fig. 3A–J). Also, for all

the measurements, *Reep6*$^{E5/+}$ and *Reep6*$^{+/-}$ consistently showed no differences. Interestingly, at 4 weeks postnatal, *Reep6*$^{E5/E5}$ showed a reduction of a-wave amplitude, however, it showed a normal b-wave, compared with *Reep6*$^{E5/+}$ and *Reep6*$^{+/-}$ (Fig. 3A–E). At 16 weeks postnatal, the a-wave of *Reep6*$^{E5/E5}$ were also reduced to the level similar to that of *Reep6*$^{E5/-}$ and *Reep6*$^{-/-}$ (Fig. 3F–J), whereas the b-wave of *Reep6*$^{E5/E5}$, also showed a decreased appearance compared with Reep6$^{E5/+}$ and Reep6$^{+/-}$. At 16 weeks, the b-wave of *Reep6*$^{E5/E5}$ showed no statistical significance with *Reep6*$^{+/-}$ ($P = 0.12$) or *Reep6*$^{-/-}$ ($P = 0.15$), suggesting that it was at an intermediate level. From the ERG analysis, we conclude that *Reep6*$^{E5/E5}$ and *Reep6*$^{E5/-}$ mice both showed severe visual defects.

To confirm the observations from the ERGs, histological analysis was performed on the retina tissue at the age of 16 weeks postnatal. Paraffin-embedded retinal cross-sections were stained with hematoxylin and eosin (H&E). Sections close to the center of the eye, with the optic nerve present in the section, were analyzed (Fig. 4A–F, Supplementary Material, Fig. S1). The thickness of the ONL was measured, from the site of optic nerve to either edge of the retina every 250 μm. Consistent with the ERG recording results, the *Reep6*$^{E5/E5}$ and *Reep6*$^{E5/-}$ mice displayed significant thinning of the ONL. The ONL thickness of *Reep6*$^{E5/E5}$ and *Reep6*$^{E5/-}$ were comparable to, if not lower than, that of *Reep6*$^{-/-}$. As expected, *Reep6*$^{E5/+}$ showed normal ONL thickness similar to *Reep6*$^{+/-}$ (Fig. 4F). Thus, histological analysis results demonstrated that the *Reep6*$^{E5/E5}$ and *Reep6*$^{E5/-}$ mice had a photoreceptor degeneration phenotype and their severity was similar to *Reep6*$^{-/-}$.

Taken together, the *Reep6*^{E5} allele results in severe loss of function phenotype in the retina, indicating that the Reep6.1 isoform is required for normal visual function and photoreceptor survival. Substitution of *Reep6.1* with *Reep6.2* at the endogenous level in the retina, as shown in *Reep6*$^{E5/E5}$, was not sufficient to maintain its normal function. On the other hand, *Reep6*$^{E5/+}$ retina demonstrated normal function, indicating that the Reep6.2 protein did not show harmful effects in the retina at this level.

Reep6.2 overexpression was not able to rescue the photoreceptor degeneration in *Reep6*$^{-/-}$

Results described above strongly suggest that the activity of *Reep6.1* and *Reep6.2* in photoreceptor cells is not equivalent. However, it is possible that the activity of *Reep6.2* may be lower than that of *Reep6.1* in photoreceptor cells, resulting in defects when the *Reep6.1* isoform is replaced by the *Reep6.2* isoform at the endogenous level. To test this hypothesis, a rescue experiment was performed by overexpressing *Reep6.2* isoform in the *Reep6*$^{-/-}$ retina. AAV8-based gene delivery administered by subretinal injection at 3 weeks postnatal was used to overexpress *Reep6.2* cDNA in *Reep6*$^{-/-}$ mouse retina. As a control, *Reep6.1* isoform was delivered with the same vector and same method in parallel. Also, to control for the possible damaging effect of subretinal injection, we injected the same amount of PBS to *Reep6*$^{+/+}$ and *Reep6*$^{-/-}$ mice. For both AAV vectors, the Reep6 protein was fused with a 3x tandem FLAG tag, at the N-terminus. Tissues were collected at 16 weeks postnatal. IF staining confirmed the overexpression of *Reep6.2* and *Reep6.1* in the injected mice retina (Fig. 5). Histological analysis was then performed on the injected eyes using the same strategy as defined previously. The ONL thickness among 4 conditions were compared, including *Reep6*$^{+/+}$ and *Reep6*$^{-/-}$ with PBS injection, and *Reep6*$^{-/-}$ injected with *Reep6.1* and *Reep6.2*, respectively. Three biological replicates were used for each group. Consistent with a previous study (19), rescue of ONL thickness is observed when treated *Reep6.1* (Fig. 6A–E). In contrast, no rescue was observed when *Reep6.2* cDNA is injected into *Reep6*$^{-/-}$ retina (Fig. 6A–E). These results further support the idea that *Reep6.1* has a distinct function in photoreceptor cells that cannot be compensated by a high level of *Reep6.2* expression.

Discussion

Dysregulation of mRNA splicing is one of the causes of inherited retinal diseases (IRDs). Mutations in the splicing sites of multiple IRD genes, such as *RHO* and *USH2A*, have been reported in retinal degeneration patients (20–24). Also, mutations in splicing factors such as *PRPF31*, *PRPF8* and *PRPF3*, etc. also cause retinal degeneration in humans (25–29). Compared with these two scenarios of abnormal splicing, much less have been reported regarding abnormalities in alternatively spliced isoforms or alternative exons. One of the rare examples is that of a mutation causing the skip of a retinal specific exon in *BBS8* caused retinal degeneration in humans (30). An example with validation in mouse models is that overexpression of a canonical isoform of *Rpgr*, namely *Rpgr*$^{e1\text{-}19}$, led to retinal degeneration while overexpression of *Rpgr*^{ORF15}, a retinal specific isoform, was tolerable (31). Mutations in alternative exons of *Rpgr* were reported to cause IRD in humans, highlighting their importance in normal function. However, because of the complexity of the *Rpgr* gene, the previous study crossed an isoform-specific transgenic mouse line with the full knockout line, which led to less control of the protein expression levels. Unlike *Rpgr*, *Reep6* has only one isoform expressed in adult mouse rod cells, and the two possible *Reep6* isoforms only differ by a single exon. This allows us to generate an alternative exon knockout mouse to directly substitute one isoform for the other, while retaining the intrinsic expression level.

Functional differences between gene splicing isoforms have been proposed and studied at different scales and levels. However, the number of studies involving a direct comparison between isoforms *in vivo* is limited. In this report, we performed both *in vivo* loss of function and overexpression studies and demonstrated that, consistent with the tissue-specific expression pattern, the retinal-specific isoform *Reep6.1* is required for rod cell survival. The distinct function between the *Reep6.1* and *Reep6.2* is not due to expression level, as overexpression of *Reep6.2* cannot substitute for *Reep6.1*. This alternative exon 5, interestingly, is not required for *Reep6* function in other tissues. In one case, we have shown that the Reep6 protein is required in the testis of male mice for fertility (32) and both *Reep6.1* and *Reep6.2* were expressed in the mouse testis. Curiously, full knockout of *Reep6* caused complete infertility in male mice. However, in the *Reep6*$^{E5/E5}$ model, which has *Reep6.2* only, the male mice are fertile (data not shown), which supports that *Reep6.1* is dispensable in the testis when *Reep6.2* is present. Thus, our study reveals an interesting example where the tissue-specific isoform correlates well with its tissue-specific function *in vivo*.

To generate a *Reep6.1* isoform-specific knockout, the *Reep6*^{E5} allele is generated by deleting the entire exon5 with some flanking intronic sequence. Therefore, the allele with deletion might affect the proper transcription of the *Reep6.2* isoform. However, this is unlikely given the following observations. First, a comparable *Reep6.2* transcript has been detected in the *Reep6*$^{E5/+}$ mouse retina (Fig. 1D). Second, consistent with the mRNA level, a high level of *Reep6.2* protein is produced by the *Reep6*^{E5} allele based on both IF and western blots (Fig. 1A and E). Finally, overexpression

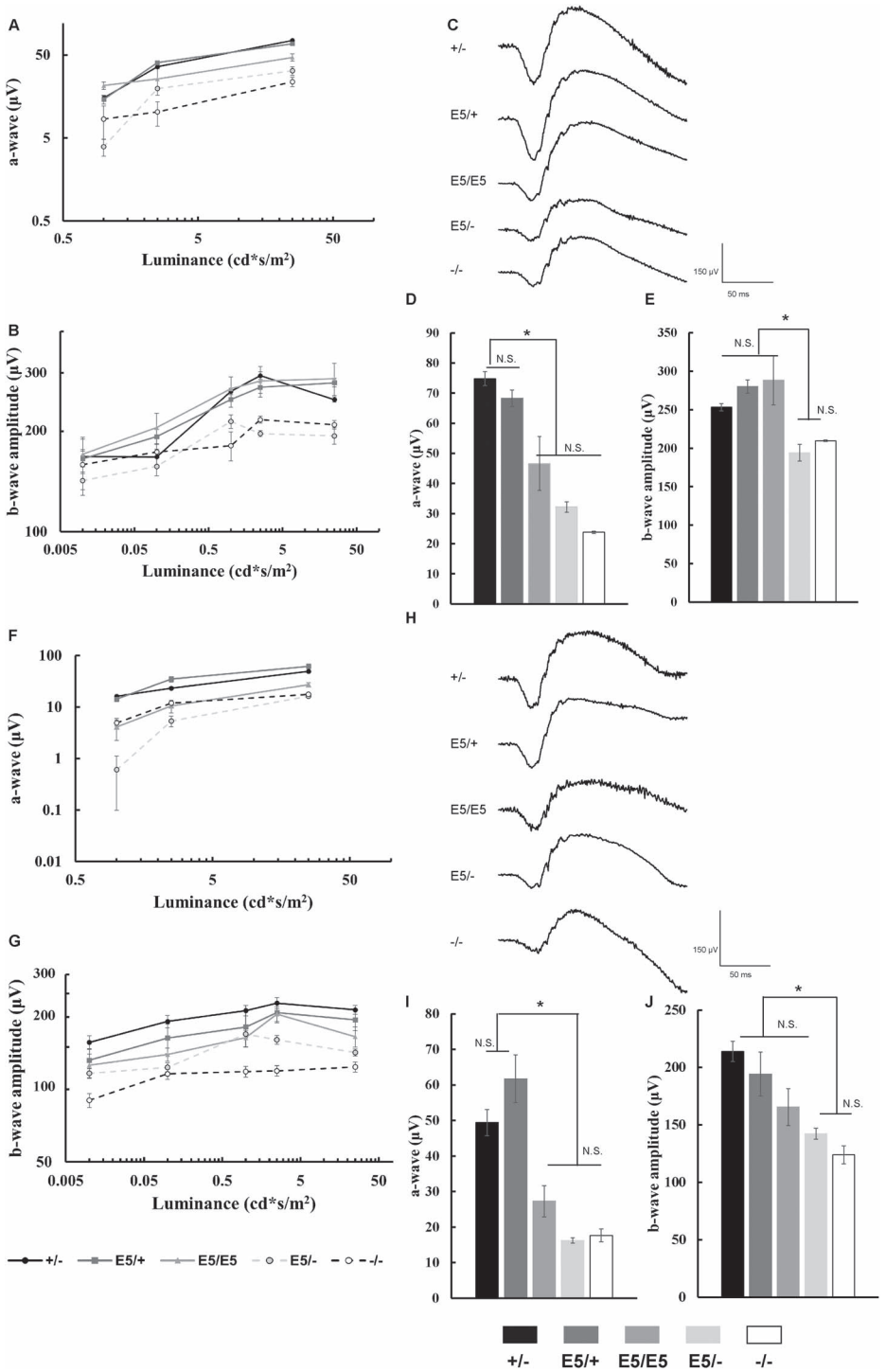

Figure 3. ERG recording of *Reep6*$^{E5/E5}$, *Reep6*$^{E5/-}$, *Reep6*$^{E5/+}$, *Reep6*$^{+/-}$ and *Reep6*$^{-/-}$ in different time points. (**A**) Scotopic a-wave measurements for mice of 4 weeks old ($N = 4, 6, 6, 7, 3$, respectively) along different stimulation luminance. (**B**) Scotopic b-wave measurements for mice of 4 weeks old ($N = 4, 6, 6, 7, 3$, respectively) along different stimulation luminance. (**C**) Representative raw ERG data for mice of 4 weeks old. (**D**) Scotopic a-wave measurements for mice of 4 weeks old ($N = 4, 6, 6, 7, 3$, respectively) at 25 cd∗s/m^2. (**E**) Scotopic b-wave measurements for mice of 4 weeks old ($N = 4, 6, 6, 7, 3$, respectively) at 25 cd∗s/m^2. (**F**) Scotopic a-wave amplifications for mice of 16 weeks old ($N = 5, 7, 4, 5, 5$, respectively) along different stimulation luminance. (**G**) Scotopic b-wave amplifications for mice of 16 weeks old ($N = 5, 7, 4, 5, 5$, respectively) along different stimulation luminance. (**H**) Representative raw ERG data for mice of 16 weeks old. (**I**) Scotopic a-wave amplifications for mice of 16 weeks old ($N = 5, 7, 4, 5, 5$, respectively) at 25 cd∗s/m^2. (**G**) Scotopic b-wave amplifications for mice of 16 weeks old ($N = 5, 7, 4, 5, 5$, respectively) at 25 cd∗s/m^2. Asterisk denotes P-value < 0.05. The legend of A, B, F, and G are the same one in bottom left; the legend of D, E, I, and J are the same in bottom right.

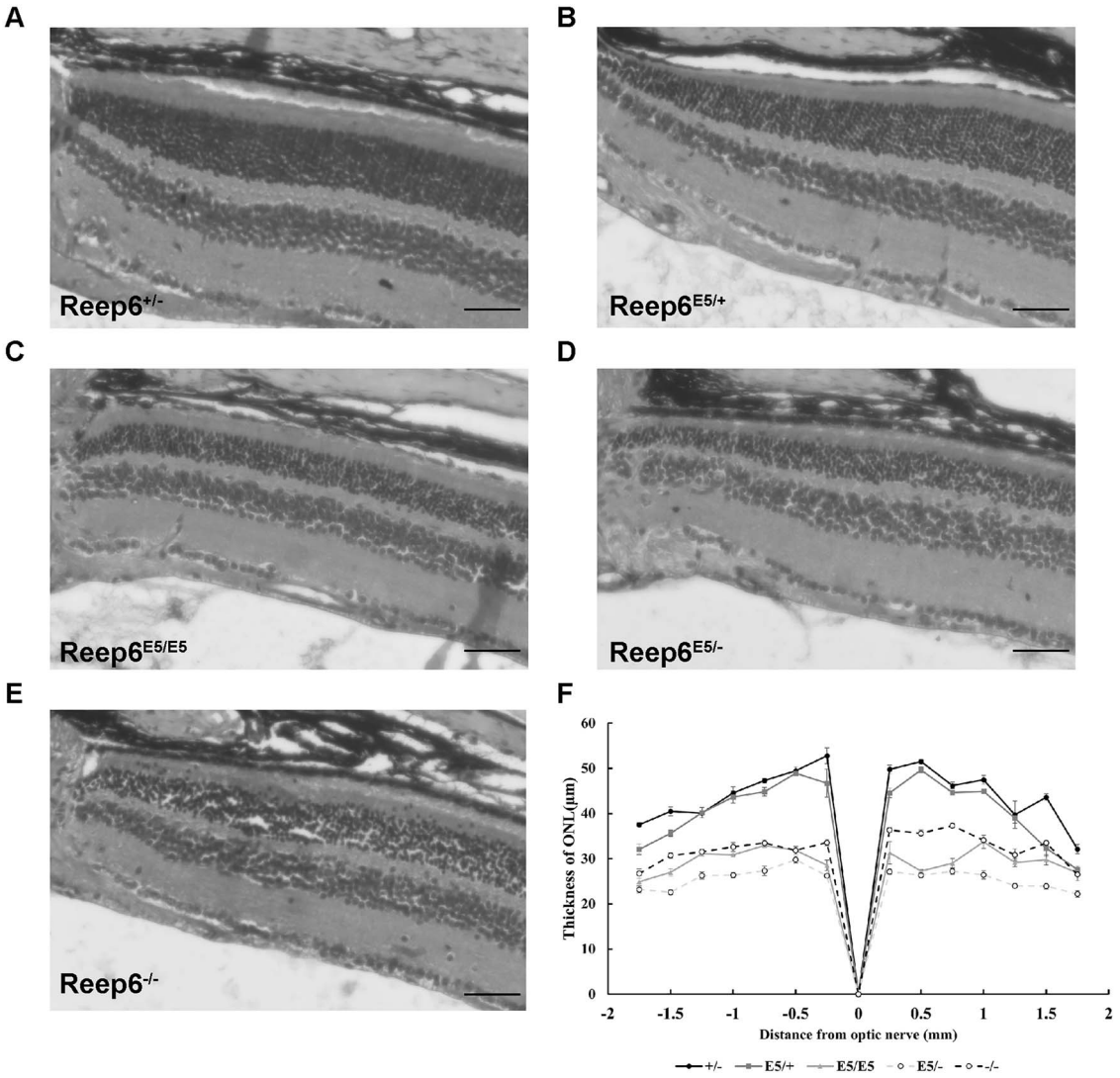

Figure 4. Histology of *Reep6*$^{+/-}$, *Reep6*$^{E5/+}$, *Reep6*$^{E5/E5}$, *Reep6*$^{E5/-}$ and *Reep6*$^{-/-}$ at 16 weeks old time point. (**A–E**) Histology of *Reep6*$^{+/-}$, *Reep6*$^{E5/+}$, *Reep6*$^{E5/E5}$, *Reep6*$^{E5/-}$ and *Reep6*$^{-/-}$ at 16 weeks old time point, respectively. The sections include optic nerves were selected to ensure the central location. Scale bar = 50 μm. (**F**) ONL thickness plotting for *Reep6*$^{+/-}$, *Reep6*$^{E5/+}$, *Reep6*$^{E5/E5}$, *Reep6*$^{E5/-}$ and *Reep6*$^{-/-}$ retina at 16 weeks old time point. Thickness was measured from optic nerve (set as center) to sides at 0.25 mm interval ($N = 3$ for all groups).

of *Reep6.2* is not sufficient to rescue the *Reep6* knock out retina phenotype, providing additional evidence that the level of *Reep6* is not the major cause of photoreceptor degeneration observed in the *Reep6*$^{E5/E5}$ retina.

Through the phenotype assessment among mice with different genotypes, we noticed that although neither of the *Reep6*$^{E5/E5}$ and *Reep6*$^{E5/-}$ mice had the Reep6.1 protein, their physiological phenotypes were not the same, reflected by the ERG data. Notably, the b-wave of *Reep6*$^{E5/E5}$ mice was normal at 4 weeks and significantly higher than that of *Reep6*$^{E5/-}$, however, at 16 weeks, they showed no differences according to statistical test. Although *Reep6*$^{E5/E5}$ b-wave showed no differences compared with Reep6$^{+/-}$ at 4 months, there was a clear decreasing trend. Besides, the average a-wave measurement of the *Reep6*$^{E5/E5}$ was consistently higher than the *Reep6*$^{E5/-}$ in both time points. All these results reflected that the *Reep6*$^{E5/E5}$ showed a less severe phenotype than *Reep6*$^{E5/-}$, and *Reep6*$^{-/-}$. One possible explanation of the observation was that the Reep6.2 protein could partially retain some functional aspects of the Reep6 protein in the retina, and this aspect could be related to the amount of the protein. It was previously reported that the Reep6 protein could participate in synaptic functions (16), which could be reflected in b-wave amplitudes. Although the Reep6.2 protein might be not as potent as Reep6.1 in this aspect, the residual potency was able to delay the worsen of synaptic functions in *Reep6*$^{E5/E5}$ mice, compared with *Reep6*$^{E5/-}$ and *Reep6*$^{-/-}$. On the other hand, supplying the retina with Reep6.1 for the *Reep6*$^{-/-}$ mice could rescue the degeneration, whereas supplement of Reep6.2 could not. This indicated that Reep6 might act as a protein with versatility in the retina, which caused that outcome that Reep6.2 could not substitute Reep6.1 and reverse the degeneration. Further studies are needed to decipher the functional complexity of the Reep6 protein in the retina.

Our study suggests that the C-terminus of the Reep6 protein containing exon 5 is important for its function in rod photoreceptor cells. The mouse Reep6.1 protein contains 201 amino acids, including 29 amino acids encoded by exon 5. The Reep6 protein shares considerable homology with a yeast protein, Yop1p,

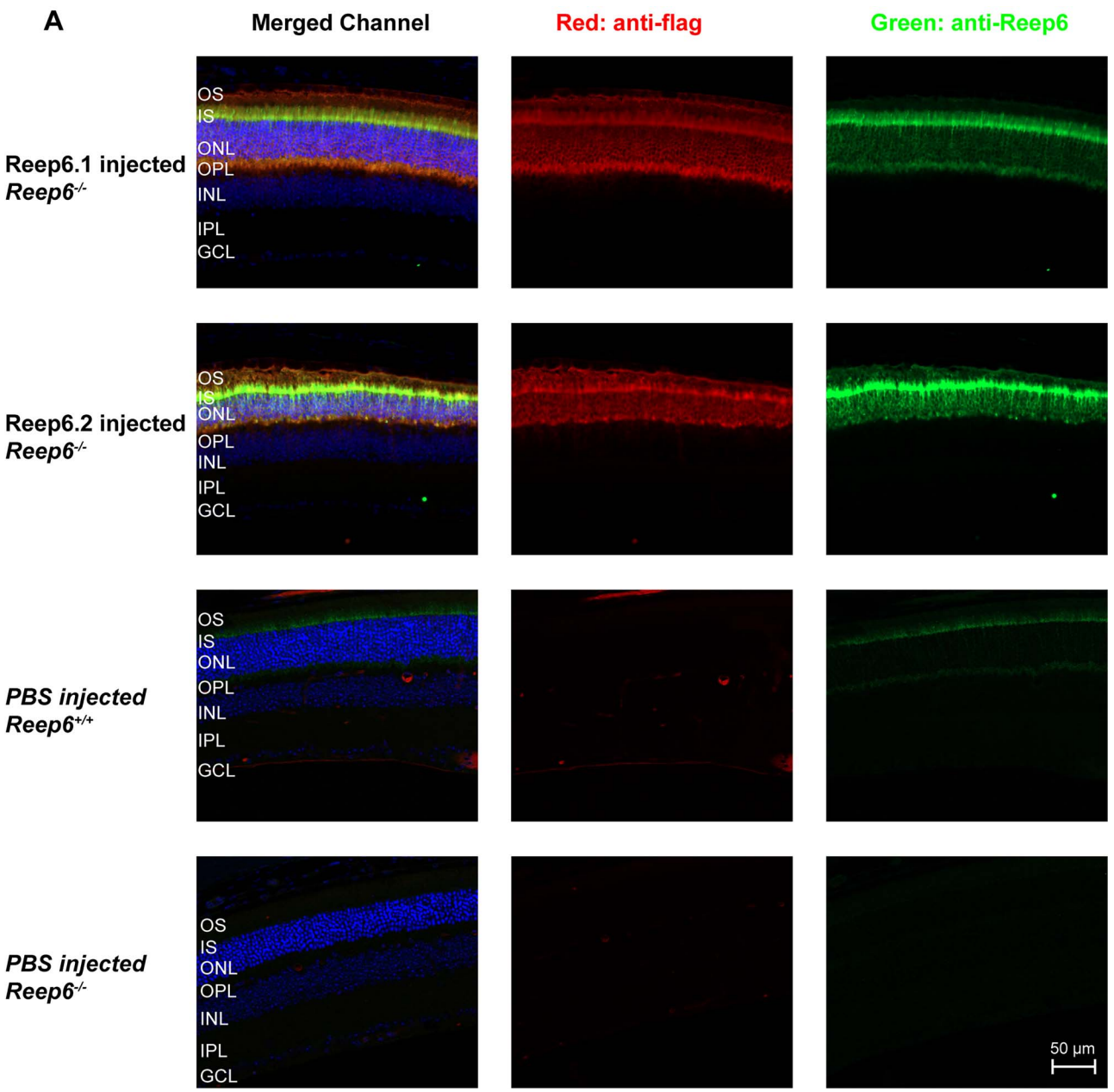

Figure 5. Immunofluorescence staining to confirm *Reep6* expression in *Reep6.1*/*Reep6.2* injected *Reep6*$^{-/-}$ mouse retina. The four rows are for *Reep6.1*-AAV injected *Reep6*$^{-/-}$, *Reep6.2*-AAV injected *Reep6*$^{-/-}$, *Reep6*$^{+/+}$ injected with PBS and *Reep6*$^{-/-}$ injected with PBS, from top to bottom.

whose structure-function relationship has been well studied (33,34). Previous studies reported that an N-terminal region of Yop1p (position 36–151) forms two short-helical hairpins and one amphipathic helix which contributes to the stabilization of the ER membrane curvature (33–35). This region is conserved among mouse Reep protein family members (Reep1–Reep6) and human Reep6 protein, indicating a conserved structure and function (Supplementary Material, Fig. S2). The corresponding region in mouse Reep6 shares 39% identity and 63% similarity with Yop1p. The C-terminus of the Reep6 (148–201 for Reep6.1 and 148–174 for Reep6.2) is less conserved and predicted to be a cytosolic region. The function of the C-terminal cytosolic region of the Reep protein family has not been well studied. Previous studies of Reep1 suggest its C-terminus interacts with microtubules (36,37). In our study, since the only difference between Reep6.1 and Reep6.2 lies in the C-terminus region, we demonstrate that although less conserved, this region has a critical function. Further study of the C-terminus domain function in the context of photoreceptor survival will likely provide important insights on tissue-specific function of the REEP/Yop1p family proteins.

In summary, using *Reep6* as an example, our study highlighted that the tissue-specific alternative exon could have indispensable functions for maintaining a normal tissue function.

Materials and Methods

Generation of *Reep6*^{E5} mice

CRISPR system was used to generate the *Reep6*^{E5} mouse. sgRNA target site was designed with UCSC tools. To obtain the exon

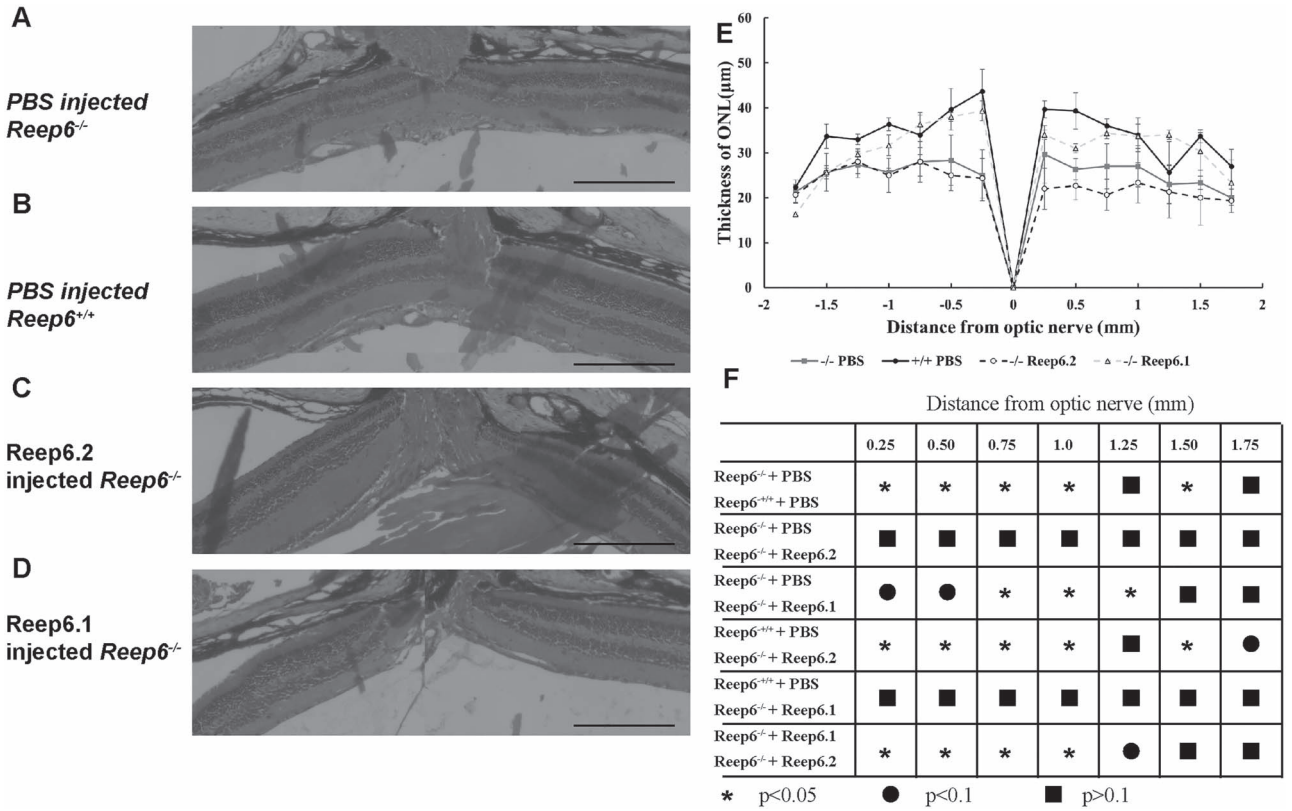

Figure 6. Histology of *Reep6*$^{-/-}$ injected with PBS, *Reep6*$^{+/+}$ injected with PBS, *Reep6.2*-AAV injected *Reep6*$^{-/-}$ and *Reep6.1*-AAV injected *Reep6*$^{-/-}$, at 16 weeks postnatal. (13 weeks post-injection). (**A–D**) Histology of *Reep6*$^{-/-}$ injected with PBS, *Reep6*$^{+/+}$ injected with PBS, *Reep6.2*-AAV injected *Reep6*$^{-/-}$ and *Reep6.1*-AAV injected *Reep6*$^{-/-}$, at 16 weeks postnatal. Scale bar = 200 μm. (**E**) ONL thickness plotting for *Reep6.1* injected *Reep6*$^{-/-}$, *Reep6.2* injected *Reep6*$^{-/-}$, *Reep6*$^{+/-}$ and *Reep6*$^{-/-}$ retina at 16 weeks old time point. Thickness was measured from optic nerve (set as center) to sides at 0.25 mm interval ($N = 3$ for all groups). (**F**) Results of the statistical test to compare between each two groups. Student's *t*-test was performed for each comparison at each distance to center. Asterisk denotes *P*-value < 0.05; circle denotes *P*-value between 0.05 and 0.1; and square denotes *P*-value > 0.1.

deletion allele, two sgRNAs were designed at upstream and downstream positions of murine *Reep6* exon 5 (upstream: CCCAGAAGCAAGATAGGGCG; downstream: CCTGCACATTTTGCTCCTCG). Cas9 mRNA and sgRNAs were then injected to mice embryos at the one-cell stage through microinjection (Cas9: 40 ng/μl and sgRNA: 10 ng/μl each). PCR-based genotype was used to test the genotype of the *Reep6*^{E5} mouse. PCR primers were: Forward: TAGCTAAGCCTCTCTCCCGA; Reverse: AAGAATGTGGTGTCAGCCCT. The PCR products of WT and *Reep6*^{E5} alleles were 700 and 260 bp, respectively.

All animals for this project were handled, fed on a standard diet and housed in a 12 h light to 12 h dark cycle. Animal experiments were approved by Institutional Animal Care and Use Committee of Baylor College of Medicine.

Electroretinogram

Mice were dark-adapted for 12 h prior to ERG recording. Before recording, each mouse was anesthetized with an anesthesia cocktail [ketamine (22 mg/kg), xylazine (4.4 mg/kg) and acepromazine (0.37 mg/kg)] through intraperitoneal injection. Afterward, each eye was treated with a series of tropicamide (1%) and phenylephrine (2.5%) solutions. The cornea was anesthetized with proparacaine (1%) before Goniosoft was applied to enhance the cornea-electrode contact.

For all the mice tested, scotopic ERG was performed at six flash intensities: −24, −14, −4, 0 and 10 dB (0.01, 0.1, 1, 2.5 and 25 cd∗s/m^2). The LKC UTAS Visual Diagnostic System and EMWIN software (LKC Technologies, Gaithersburg, MD) was utilized to digitize and store the recordings. A custom Matlab code was used to measure the amplitudes b-waves (from the a-wave trough to the positive deflection peak). To focus on the rod cell driven sensitivity to light stimulus, we did not use the full a-wave amplitude as the a-wave measurement, but instead measured the a-wave leading edge at 7 ms point. The ERG wave amplitude data were then analyzed and plotted using Microsoft Excel.

Mouse eye tissue processing and sectioning

All the H&E staining and IF staining experiments were performed on paraffin-embedded sections described further.

Enucleated mouse eyes were fixed overnight with freshly-prepared Davidson's fixative (2, 40% Formaldehyde, 35% ethanol, 10% acetic acid and 53% H_2O) at 4°C. The fixed eyes were then washed with PBS buffer twice followed by dehydration using an ethanol series (50, 70, 95 and 100%). The washing and dehydration were all processed at 4°C with mild shaking. The eyes were then washed with xylene in a fume hood twice, 1 h each, at room temperature. Afterward, the eyes were transferred to a pre-warmed 50% xylene/50% paraffin mix at 60°C for 1 h and then to 100% paraffin for an overnight incubation. The eyes were then embedded in paraffin on the next day. Paraffin-embedded tissue blocks were sectioned at 7 μm thickness.

H&E staining and measurement of ONL thickness

Paraffin sections were dewaxed with two xylene washes at room temperature for 40 and 20 min, respectively. The dewaxed sections were rehydrated with an ethanol series (100, 95, 70 and 50%) and then 100% H_2O for 5 min each. Then the sections were immersed with Hematoxylin (Harris Modified Hematoxylin, 157 070 Fisher Chemical, Waltham, MA, United states) for 30 s and then washed with H_2O three times for 2 min each. Afterward, the sections were immersed with Eosin (Eosin Y Phloxine B solution, 26 051-21, Electron Microscopy Sciences, Hatfield, PA, United States) for 45 s and then washed with H_2O three times, 2 min each. Then the sections were dehydrated with an ethanol series (50, 70, 95 and 100%), 3 min each, followed by two xylene washes, 15 min each. Finally, the slides were air-dried in a fume hood for 10 min, before they were covered with Fisher Chemical Permount mountant, and coverslipped.

H&E stained slides were visualized with Zeiss Axio Imager M2m under brightfield. For quantification of ONL thickness, tilling method was used to acquire the image of a whole section under 20× magnification. The ONL thickness was then measured with ImageJ. Distances were defined with the scale bar. The optic nerve site was set as the center and the measurement was performed from the center to both sides with a 250 μm interval. The data were then analyzed using Microsoft Excel.

IF staining

Multiple PBS washes were used in this experiment and all of them were at room temperature for 5 min.

Paraffin sections were dewaxed using two xylene washes at room temperature for 40 and 20 min, respectively. The dewaxed sections were rehydrated with ethanol series (100, 95, 70 and 50%) and then 100% H_2O, 5 min each. Antigen retrieval was performed to the sections using a sodium-citrate buffer, pH 6.0, in a 100°C water bath for 30 min. Then, the slides were washed in PBS three times. The sections were blocked with the NGST buffer (10% normal goat serum and 0.1% Triton X-100 in PBS) in a humidifying box at room temperature for 1 h. Primary antibody was diluted in NGST buffer and applied to sections. Primary antibody incubation was at 4°C, overnight. On the next day, the sections were washed with PBS three times and then treated with secondary antibody. Secondary antibody was also diluted with the NGST buffer, and the incubation was at room temperature for 1 h. After another three PBS washes, DAPI was applied to sections for 10 min. Then the sections were washed in PBS twice and air-dried. Finally, the sections were coated with Invitrogen (Carlsbad, CA, United States) Prolong Gold and coverslipped. IF stained slides were visualized with Zeiss Axio Imager M2m under certain channels.

The primary antibodies used were: anti-Reep6 [a kind gift from Dr Anand Swaroop (18), 1: 500 dilution]; anti-FLAG (SigmaAldrich, St.Louis, MO, United States; M2 clone, F3165, 1:500 dilution).

Western blot

The mouse retina was collected by dissecting freshly enucleated eyes in PBS. Each retina was put in a separate tube and dissociated with 75 μl of Dissociation Buffer (RIPA buffer with 1× protease inhibitor cocktail, Roche) following extensive trituration. Then, 25 μl of LDS loading buffer (NP0008 Invitrogen) was added into each sample. Each sample was heated at 42°C for 15 min before storage at −20°C.

Samples and protein markers (LC5615, Invitrogen, Carlsbad, CA, United States) were loaded on 4–20% Tris–Glycine gel (XV04200PK20 invitrogen, Carlsbad, CA, United States) and the gel was run under a constant 100V voltage. The protein on the gel was then wet-transferred to a nitrocellulose membrane with Tris–Glycine buffer containing 10% methanol, in a constant 250 mA current for 1 h in ice-cold water bath. The membrane was then blocked in TBST buffer (2.4 g Tris-base, 8.8 g NaCl and 1 ml Tween-20 in 1 l, pH adjusted to 7.6) with 5% skim milk at room temperature for 1 h. Primary antibody diluted in the same TBST-milk buffer was then applied to the membrane and incubated at 4°C overnight. On the next day, the membrane was washed in TBST buffer three times before the secondary antibody (diluted in the TBST-milk buffer) was applied and incubated for 2 h at room temperature. The membrane was then washed in TBST buffer three times again. We then mixed the detection reagent (ThermoScientific Waltham, MA, United States, #32 106) and it was applied to the membrane for 3 min while avoiding light. The membrane was then ready to image after draining excess reagent. We used Azure 400 imager to image the membrane. The quantification of western blot results was performed with ImageJ. The measurement of protein level was the ratio between the Reep6 signal and the control (HSP90) signal of the same lane.

The primary antibodies used here were: anti-Reep6 (a kind gift from Dr Anand Swaroop, 1:1500 dilution); anti-Hsp90 (CST , Danvers, MA, United States; #4874s, 1:5000 dilution).

Subretinal injection

The subretinal injection for this project was performed as previously reported (ref). Post-natal day 21 (P21) mice were anesthetized with an anesthesia cocktail [ketamine (22 mg/kg), xylazine (4.4 mg/kg) and acepromazine (0.37 mg/kg)] by intraperitoneal injection. A shallow incision was made through the sclera with a beveled 30-gauge needle. Afterward, a syringe (Model 75 SN SYR, Hamilton, Reno, NV, United States) was inserted inside the vitreous cavity and pushed towards the back of the retina. The AAV solution (1 μl) was then injected to the subretinal space manually. For each mouse, both its left and right eyes were injected, one with AAV-Reep6.1 and the other with AAV-Reep6.2, assigned randomly to the left and right eye. PBS (1 μl for each eye) were injected to wild type or Reep6$^{-/-}$ mice as injection control.

The vector used for packaging AAV contains a GRK promoter to force strong gene expression in the retina. AAV-Reep6.1 was also reported in our previous study. AAV used for this study was produced by the Gene Vector Core at Baylor College of Medicine. The titer for AAV-Reep6.1 was 7E12 (g.c/ml) and AAV-Reep6.2 was 1E13 (g.c/ml).

RNA-sequencing data analysis

The RNA-seq data of human retina (SRR5225761, SRR5225765, SRR5225769, SRR5225773, SRR5225777, SRR5225781, SRR5225785 and SRR5225789) were obtained from NCBI SRA. The RNA-seq data of human brain frontal cortex BA9, brain cerebellum, skin of sun exposed lower leg, skeletal muscle, kidney cortex, whole blood, testis and adipose subcutaneous were collected from dbGap (https://www.ncbi.nlm.nih.gov/projects/gap/cgi-bin/study.cgi?study_id=phs000424.v7.p2), and the RNA-seq data of four individuals were downloaded for each tissue respectively. We then aligned the RNA-seq data of each sample to the human genome (hg19) with HISAT2 (38). For each tissue type, the bam files of all the samples were merged to generate a

bigwig file, which was uploaded to UCSC genome browser for display.

Statistics

Student's *t*-test was used to compare every two groups. Error bar shows standard error in this study.

Supplementary Material

Supplementary Material is available at *HMGJ* online.

Acknowledgements

We thank Dr Anand Swaroop from the NEI for kindly sharing the anti-Reep6 antibody. We thank the Genetically Engineered Mouse Core that is partially supported by the National Institutes of Health (NIH) grant P30CA125123 at Baylor College of Medicine for generating Reep6 mouse models using CRISPR-gene editing. We thank the Gene Vector Core for packaging desired vector to AAV for achieving robust transduction efficiency.

Conflict of Interest statement. The authors have no conflicts of interest to declare.

Funding

National Institutes of Health (P30CA125123); National Eye Institute (R01EY022356, P30EY002520); Retina Research Foundation (S10OD023469 to R.C.).

References

1. Wahl, M.C., Will, C.L. and Lührmann, R. (2009) The spliceosome: design principles of a dynamic RNP machine. *Cell*, **136**, 701–718.
2. Kelemen, O., Convertini, P., Zhang, Z., Wen, Y., Shen, M., Falaleeva, M. and Stamm, S. (2013) (2013) Function of alternative splicing. Function of alternative splicing. *Gene*, **514**, 1–30.
3. Roy, B., Haupt, M. and Griffiths, L., R. (2013) Review: alternative splicing (AS) of genes as an approach for generating protein complexity. *Curr. Genomics*, **14**, 182–194.
4. Yang, X., Coulombe-Huntington, J., Kang, S., Iakoucheva, L.M., Xia, Y. and Vidal, M. (2016) Widespread expansion of protein interaction capabilities by alternative splicing. *Cell*, **164**, 805–817.
5. Matera, A. (2014) G. and Wang, Z. (2014) A day in the life of the spliceosome. A day in the life of the spliceosome. *Nat. Rev. Mol. Cell Biol.*, **15**, 108–121.
6. Lee, Y. and Rio, D.C. (2015) Mechanisms and regulation of alternative pre-mRNA splicing. *Annu. Rev. Biochem.*, **84**, 291–323.
7. Wang, E.T., Sandberg, R., Luo, S., Khrebtukova, I., Zhang, L., Mayr, C., Kingsmore, S.F., Schroth, G.P. and Burge, C.B. (2008) Alternative isoform regulation in human tissue transcriptomes. *Nature*, **456**, 470–476.
8. Wen, J., Chiba, A. and Cai, X. (2010) Computational identification of tissue-specific alternative splicing elements in mouse genes from RNA-Seq. *Nucleic Acids Res.*, **38**, 7895–7907.
9. Badr, E., ElHefnawi, M. and Heath, L.S. (2016) Computational identification of tissue-specific splicing regulatory elements in human genes from RNA-seq data. *PLoS One*, **11**, e0166978.
10. Kalsotra, A., Xiao, X., Ward, A.J., Castle, J.C., Johnson, J.M., Burge, C.B. and Cooper, T.A. (2008) A postnatal switch of CELF and MBNL proteins reprograms alternative splicing in the developing heart. *Proc. Natl. Acad. Sci. U. S. A.*, **105**, 20333–20338.
11. Su, C.-H. (2018) D, D. and Tarn, W.-Y, Alternative splicing in neurogenesis and brain development. *Front. Mol. Biosci.*, **5**, 12.
12. Zhang, X., Chen, M.H., Wu, X., Kodani, A., Fan, J., Doan, R., Ozawa, M., Ma, J., Yoshida, N., Reiter, J.F. *et al.* (2016) Cell-type-specific alternative splicing governs cell fate in the developing cerebral cortex. *Cell*, **166**, 1147–1162.e15.
13. Zhang, M., Ergin, V., Lin, L., Stork, C., Chen, L. and Zheng, S. (2019) Axonogenesis is coordinated by neuron-specific alternative splicing programming and splicing regulator PTBP2. *Neuron*, **101**, 690–706.e10.
14. Björk, S., Hurt, C.M., Ho, V.K. and Angelotti, T. (2013) REEPs are membrane shaping adapter proteins that modulate specific G protein-coupled receptor trafficking by affecting ER cargo capacity. *PLoS One*, **8**, e76366.
15. Arno, G., Agrawal, S.A., Eblimit, A., Bellingham, J., Xu, M., Wang, F., Chakarova, C., Parfitt, D.A., Lane, A., Burgoyne, T. *et al.* (2016) Mutations in REEP6 cause autosomal-recessive retinitis pigmentosa. *Am. J. Hum. Genet.*, **99**, 1305–1315.
16. Veleri, S., Nellissery, J., Mishra, B., Manjunath, S.H., Brooks, M.J., Dong, L., Nagashima, K., Qian, H., Gao, C., Sergeev, Y.V. *et al.* (2017) REEP6 mediates trafficking of a subset of Clathrin-coated vesicles and is critical for rod photoreceptor function and survival. *Hum. Mol. Genet.*, **26**, 2218–2230.
17. Agrawal, S.A., Burgoyne, T., Eblimit, A., Bellingham, J., Parfitt, D.A., Lane, A., Nichols, R., Asomugha, C., Hayes, M.J., Munro, P.M. *et al.* (2017) REEP6 deficiency leads to retinal degeneration through disruption of ER homeostasis and protein trafficking. *Hum. Mol. Genet.*, **26**, 2667–2677.
18. Hao, H., Veleri, S., Sun, B., Kim, D.S., Keeley, P.W., Kim, J.-W., Yang, H.-J., Yadav, S.P., Manjunath, S.H., Sood, R. *et al.* (2014) Regulation of a novel isoform of Receptor Expression Enhancing Protein REEP6 in rod photoreceptors by bZIP transcription factor NRL. *Hum. Mol. Genet.*, **23**, 4260–4271.
19. Zaneveld, S. A., Eblimit, A., Liang, Q., Bertrand, R., Wu, N., Liu, H., Nguyen, Q., Zaneveld, J., Wang, K., Li, Y., *et al.* (2018) Gene therapy rescues retinal degeneration in receptor expression-enhancing protein 6 mutant Mice. *Hum. Gene Ther.*, **30**, 302–315.
20. Liu, M.M., Zack, D.J. and Zack, D. (2013) Alternative splicing and retinal degeneration. *Clin. Genet.*, **84**, 142–149.
21. Whitehead, J.L., Bell, C., Converse, C.A., Hammer, H.M. and Haites, N.E. (1998) Rhodopsin splice site sequence changes in retinitis pigmentosa and their effect at the mRNA level. *Hum. Mutat.*, **11**, S295–S297.
22. Gamundi, M.J., Hernan, I., Muntanyola, M., Maseras, M., López-Romero, P., Álvarez, R., Dopazo, A., Borrego, S. and Carballo, M. (2008) Transcriptional expression of *cis* -acting and *trans* -acting splicing mutations cause autosomal dominant retinitis pigmentosa. *Hum. Mutat.*, **29**, 869–878.
23. Le Guédard-Méreuze, S., Vaché, C., Baux, D., Faugère, V., Larrieu, L., Abadie, C., Janecke, A., Claustres, M., Roux, A.F. and Tuffery-Giraud, S. (2010) Ex vivo splicing assays of mutations at noncanonical positions of splice sites in USHER genes. *Hum. Mutat.*, **31**, 347–355.
24. Jaijo, T., Aller, E., Aparisi, M.J., García-García, G., Hernan, I., Gamundi, M.J., Nájera, C., Carballo, M. and Millán, J.M. (2011) Functional analysis of splicing mutations in MYO7A and USH2A genes. *Clin. Genet.*, **79**, 282–288.

25. Al-Maghtheh, M., Vithana, E., Tarttelin, E., Jay, M., Evans, K., Moore, T., Bhattacharya, S. and Inglehearn, C.F. (1996) Evidence for a major retinitis pigmentosa locus on 19q13.4 (RP11), and association with a unique bimodal expressivity phenotype. *Am. J. Hum. Genet.*, **59**, 864–871.
26. Vithana, E.N., Abu-Safieh, L., Allen, M.J., Carey, A., Papaioannou, M., Chakarova, C., Al-Maghtheh, M., Ebenezer, N.D., Willis, C., Moore, A.T. *et al.* (2001) A human homolog of yeast pre-mRNA splicing gene, PRP31, underlies autosomal dominant retinitis pigmentosa on chromosome 19q13.4 (RP11). *Mol. Cell*, **8**, 375–381.
27. Mckie, A.B., Mchale, J.C., Keen, T.J., Tarttelin, E.E., Goliath, R., Van Lith-Verhoeven, J.J.C., Greenberg, J., Ramesar, R.S., Hoyng, C.B., Cremers, F.P.M. *et al.* (2001) Mutations in the pre-mRNA splicing factor gene PRPC8 in autosomal dominant retinitis pigmentosa (RP13). *Hum. Mol. Genet.*, **10**, 1555–1562.
28. Chakarova, C.F., Hims, M.M., Bolz, H., Abu-Safieh, L., Patel, R.J., Papaioannou, M.G., Inglehearn, C.F., Keen, T.J., Willis, C., Moore, A.T. *et al.* (2002, 2002) Mutations in HPRP3, a third member of pre-mRNA splicing factor genes, implicated in autosomal dominant retinitis pigmentosa. *Hum. Mol. Genet.*, **11**, 87–92.
29. Martínez-Gimeno, M., José Gamundi, M., Hernan, I., Maseras, M., Millá, E., Ayuso, C., García-Sandoval, B., Beneyto, M., Vilela, C., Baiget, M. *et al.* (2003) Mutations in the pre-mRNA splicing-factor genes PRPF3, PRPF8, and PRPF31 in Spanish families with autosomal dominant retinitis pigmentosa. *Investig. Ophthalmol. Vis. Sci.*, **44**, 2171–2177.
30. Riazuddin, S.A., Iqbal, M., Wang, Y., Masuda, T., Chen, Y., Bowne, S., Sullivan, L.S., Waseem, N.H., Bhattacharya, S., Daiger, S.P. *et al.* A splice-site mutation in a retina-specific exon of BBS8 causes nonsyndromic retinitis pigmentosa. *Am J Hum Genet.*, **86**, 805–812.
31. Neidhardt, J., Glaus, E., Barthelmes, D., Zeitz, C., Fleischhauer, J. and Berger, W. (2007) Identification and characterization of a novel RPGR isoform in human retina. *Hum. Mutat.*, **28**, 797–807.
32. Devlin, D.J., Agrawal Zaneveld, S., Nozawa, K., Han, X., Moye, A.R., Liang, Q., Harnish, J.M., Matzuk, M.M. and Chen, R. Knockout of mouse receptor accessory protein 6 leads to sperm function and morphology defects. *Biol. Reprod.*, **102**, 1234–1247.
33. Voeltz, G.K., Prinz, W.A., Shibata, Y., Rist, J.M. and Rapoport, T.A. (2006) A class of membrane proteins shaping the tubular endoplasmic reticulum. *Cell*, **124**, 573–586.
34. Shibata, Y., Voss, C., Rist, J.M., Hu, J., Rapoport, T.A., Prinz, W.A. and Voeltz, G.K. (2008) The reticulon and DP1/Yop1p proteins form immobile oligomers in the tubular endoplasmic reticulum. *J. Biol. Chem.*, **283**, 18892–18904.
35. Brady, J.P., Claridge, J.K., Smith, P.G. and Schnell, J.R. (2015) A conserved amphipathic helix is required for membrane tubule formation by Yop1p. *Proc. Natl. Acad. Sci. U. S. A.*, **112**, E639–E648.
36. Park, S.H., Zhu, P.-P., Parker, R.L. and Blackstone, C. (2010) Hereditary spastic paraplegia proteins REEP1, spastin, and atlastin-1 coordinate microtubule interactions with the tubular ER network. *J. Clin. Invest.*, **120**, 1097–1110.
37. Beetz, C., Koch, N., Khundadze, M., Zimmer, G., Nietzsche, S., Hertel, N., Huebner, A.-K., Mumtaz, R., Schweizer, M., Dirren, E. *et al.* (2013) A spastic paraplegia mouse model reveals REEP1-dependent ER shaping. *J. Clin. Invest.*, **123**, 4273–4282.
38. Kim, D., Langmead, B. and Salzberg, S.L. (2015) HISAT: A fast spliced aligner with low memory requirements. *Nat. Methods*, **12**, 357–360.